Symmetry breaking in networks of nonlinear cavities

Koen Huybrechts, Geert Morthier, Bjorn Maes

Photonics Research Group, Department of Information Technology (INTEC)
Ghent University - IMEC
Sint-Pietersnieuwstraat 41, B-9000 Ghent
Belgium

We demonstrate symmetry breaking in ring-like networks composed of three and four coupled nonlinear cavities, such as photonic crystal resonators. With coupled mode theory we derive analytical conditions for the appearance of asymmetric states. The rich dynamical behaviour is further demonstrated by time-domain calculations, which show cyclical switching action that is useful for multi-stable all-optical flip-flops.

OCIS codes: 190.3270, 190.1450, 230.4555

1. Introduction

Structures with coupled nonlinear photonic cavities exhibit a rich and intricate dynamical behaviour. This opens up a whole new range of applications such as photonic reservoir computing [1], slow light engineering [2] and all-optical flip-flop operation [3]. Therefore it is important to develop clear insights into the possible states and instabilities of progressively more complex designs. By now, networks of hundreds of coupled cavities have been studied experimentally in the linear regime [4] and the next logical step is to study the effects of the non-linearities in smaller networks. Network motifs consisting of three or four nodes [5] already have a significant degree of complexity, and here our aim is to examine the nonlinear properties of such photonic cavity designs.

Symmetry breaking is a counterintuitive physical effect that describes the appearance of asymmetric states while the structure under study, and its excitation, is completely symmetric. In previous work [3,6], it was shown that two coupled nonlinear cavities can exhibit symmetry breaking: when equal power is injected on both sides of the coupled cavities, the reflected output power is different on both sides of the cavities due to non-linear effects. The symmetry breaking would not be possible in a linear structure. In this paper we couple multiple passive cavities with a Kerr-based nonlinearity in a symmetric structure. In addition, the

system is excited equally from all sides with a holding beam. We show that these symmetric setups result in different nonlinear regimes than in the case of systems with two cavities, with various kinds of asymmetric states. Furthermore, using time-domain studies in the case of three and four coupled cavities, we demonstrate multi-state flip-flop operation [7, 8]. In these cases a cyclical switching action is obtained.

Using coupled-mode theory we derive analytical conditions for the symmetry breaking detuning requirements. Our description is quite general and therefore independent of the exact implementation. The system could be implemented with compact nonlinear photonic crystal cavities [9–11] or ring resonators [12]. Recently demonstrated hybrid material systems are also a promising solution [13].

In section II, we discuss the behaviour of three cavities in a triangular configuration. Using coupled-mode theory we derive an analytical condition for symmetry breaking in this structure. Afterwards we look at the different asymmetric states under steady state conditions and we conclude by studying the dynamical behaviour with the multi-state flip-flop operation. In section III, we do the same for a configuration of four cavities: after deriving an analytical condition for symmetry breaking and discussing the steady state behaviour, we give insight in the switching between the asymmetric states.

2. Three coupled cavities

[Fig. 1 about here.]

2.A. Symmetry breaking condition

We apply coupled-mode theory on a symmetric structure consisting of three coupled nonlinear cavities as depicted in Figure 1. The time dependence of the amplitude a_i of the resonance modes of the cavities is given by [15, 16]:

$$\frac{\mathrm{d}a_1}{\mathrm{d}t} = \left[i\left(\omega_0 + \delta\omega_1\right) - \frac{1}{\tau}\right] a_1 + df_1 + db_4 + df_6 \tag{1}$$

$$\frac{\mathrm{d}a_2}{\mathrm{d}t} = \left[i\left(\omega_0 + \delta\omega_2\right) - \frac{1}{\tau}\right] a_2 + df_2 + db_5 + df_4 \tag{2}$$

$$\frac{\mathrm{d}a_3}{\mathrm{d}t} = \left[i\left(\omega_0 + \delta\omega_3\right) - \frac{1}{\tau}\right] a_3 + df_3 + db_6 + df_5 \tag{3}$$

Here f_i and b_i are the forward and backward propagating mode amplitudes in the waveguides. We assume the three cavities have the same resonant mode with center frequency ω_0 and with at least a three-fold symmetry (e.g. monopole) in order to have the same coupling d to the three waveguides. The nonlinear frequency shift due to the Kerr nonlinearity is given by

$$\delta\omega_i = \frac{-|a_i|^2}{P_0\tau^2} \tag{4}$$

with P_0 the characteristic nonlinear power of the cavity [15] and τ the lifetime of the cavity which can be related to the Q-factor as $Q = \omega_0\tau/2$. A formula for the coupling d between the waveguide modes and the cavity can be derived by applying energy conservation laws on the coupled-mode equations [16] and we find

$$d = i\sqrt{\frac{2}{3\tau}}\exp\left(i\frac{\phi}{2}\right) \tag{5}$$

Here ϕ represents the phase depending on the waveguide length and the reflection properties. For high-Q cavities and small detunings, ϕ will be quasi independent of the frequency.

The amplitudes of the forward and backward propagating waves are coupled by [17]:

$$f_4 = \exp(i\phi)b_4 + da_1 \tag{6}$$

$$b_4 = \exp(i\phi)f_4 + da_2 \tag{7}$$

Similar equations hold for the other waveguides.

The analysis will be done in the frequency domain so $\mathrm{d}/\mathrm{d}t$ will be replaced by $i\omega$ (with ω the operating frequency). The forward and backward internal waveguide amplitudes can be eliminated in equations (1-3) and we obtain:

$$\left[i\left(\omega_0 - \omega + \delta\omega_1\right) - \frac{1}{\tau}\right]a_1 + \kappa\left(2\gamma a_1 + a_2 + a_3\right) = -df_1 \tag{8}$$

$$\left[i\left(\omega_0 - \omega + \delta\omega_2\right) - \frac{1}{\tau}\right]a_2 + \kappa\left(2\gamma a_2 + a_1 + a_3\right) = -df_2 \tag{9}$$

$$\left[i\left(\omega_0 - \omega + \delta\omega_3\right) - \frac{1}{\tau}\right]a_3 + \kappa\left(2\gamma a_3 + a_1 + a_2\right) = -df_3 \tag{10}$$

with $\gamma = \exp(i\phi)$ and $\kappa = d^2/(1-\gamma^2)$. In our further analysis, we will use dimensionless cavity energies $A = -|a_1|^2/P_0\tau$, $B = -|a_2|^2/P_0\tau$ and $C = -|a_3|^2/P_0\tau$, and a dimensionless detuning $\Delta = \tau(\omega_0 - \omega)$. This detuning Δ can be expressed also in terms of the linewidth $\delta\Omega$ of the cavity mode as $\Delta = 2(\omega_0 - \omega)/\delta\Omega$. To examine the effect of symmetry breaking we assume equal input powers and phases from all sides (i.e. $f_1 = f_2 = f_3$). Elimination of f_1 in the above equations gives:

$$\left[-\frac{1}{3} + i\left(\Delta' + A\right)\right]a_1 = \left[-\frac{1}{3} + i\left(\Delta' + B\right)\right]a_2 \tag{11}$$

$$= \left[-\frac{1}{3} + i\left(\Delta' + C\right)\right]a_3 \tag{12}$$

with

$$\Delta' = \Delta - \frac{2\cos(\phi) - 1}{3\sin(\phi)} \tag{13}$$

We take the modulus squared of equation (11) and after factoring we get:

$$(A - B)\left(B^2 + (A + 2\Delta')B + A^2 + 2\Delta' A + \Delta'^2 + \frac{1}{9}\right) = 0 \tag{14}$$

A similar equation holds for the relation between A and C.

Apart from the symmetric solutions derived from the first factor ($A = B = C$), there is also the possibility of an asymmetric solution (second factor) if the detuning Δ' is chosen correctly and if the solution is stable. The factor of the asymmetric solution can be seen as a quadratic equation in B for which the discriminant has to be positive for the existence of real solutions:

$$-3A^2 - 4\Delta' A - \frac{4}{9} > 0 \tag{15}$$

This condition is fullfilled if A lies between the values

$$-\frac{2\Delta'}{3} \pm \frac{2\sqrt{9\Delta'^2 - 3}}{9} \tag{16}$$

Thus the asymmetric solution exists if $|\Delta'| > 1/\sqrt{3}$. In case of a self-focusing Kerr effect (positive nonlinearity), A is negative and therefore the condition for symmetry breaking is:

$$\Delta' > \frac{1}{\sqrt{3}} \tag{17}$$

2.B. Static solutions

By solving the coupled-mode equations under steady state conditions, we can find the static solutions as a function of the input power. In addition, a stability analysis needs to be performed to determine which of the possible states are stable, and thus excitable in experiments.

The linear stability analysis is done by evaluating the eigenvalues of the Jacobian matrix for the obtained states. Therefore we rewrite equations (1-3) into 6 ODE's where the phase and amplitude are considered separately. The elements of the Jacobian matrix are obtained by taking the derivatives of these equations to each of the variables (amplitude and phase of a_i). After evaluating this 6×6 Jacobian matrix in the possible solutions, we can determine the corresponding eigenvalues. If the real part of all these eigenvalues is negative, the system will move into the direction of the equilibrium point.

The stable output powers are depicted as a function of the input power in two different configurations where the condition for symmetry breaking (Equation 17) is fulfilled (Figure 2). One can clearly observe that besides the symmetric solution (all output powers the same and equal to P_{in}), asymmetric solutions show up for a certain range of input powers (regions I, II and III). With increasing input power, we uncover a distinctive progression through three possible symmetry breaking regimes. In region I of Figure 2a, we distinguish solutions where two out of three output powers are equal and have a higher value than the third output which is low. By increasing the input power, the two equal outputs split up (region II) and the symmetry breaking in the system is complete: all three output powers are different. This state then transforms to region III where two low output powers are equal

and the third output is high. When we change the phase ϕ, we find the bifurcation depicted in Figure 2b where the same states appear but in a different order. The parameters of the two examples are chosen in order to show the three possible regimes in a single example, but were not optimized for possible other conditions. Higher values for the detuning Δ seem to increase the extinction ratio but also moves the asymmetric regime to higher input powers. However, we did not perform extensive analysis on this matter.

[Fig. 2 about here.]

To have more insight in the symmetric solution of Figure 2a, we depict the energy of the resonant modes in the cavities as a function of the input power (Figure 3). It appears that the symmetric solution itself exhibits also a bifurcation structure. Despite this bifurcation in the cavity energies of the symmetric solutions, this asymmetry does not show up in the output powers of Figure 2 because the two branches have equal output powers (cfr. conservation of energy), but a different phase. In the lower branch, the symmetric solution becomes unstable for certain input powers and in that range the asymmetric solutions are possible. This means that we can avoid the symmetric solutions of the upper branch if we stay below the input power threshold of $P_{in} \approx 4.5P_0$. For the second case (with $\phi = 2.0$), this bistability in the symmetric solution does not show up and we find that only stable asymmetric solutions appear in the region of symmetry breaking.

[Fig. 3 about here.]

To see the influence of the parameters Δ and ϕ, we depict the appearance of the different states in Figure 4 for a constant input power of 3.0 P_0. We can clearly observe the same three regions as described before.

[Fig. 4 about here.]

2.C. Dynamic behaviour

We can study the dynamical behaviour by solving the equations 1-3 in the time domain. In the third regime of Figure 2a, it is possible to switch between asymmetric states where one of the outputs is high and the other two outputs are low. This results in multi-stable flip-flop operation [7, 8]. When a short pulse is applied to two of the three ports, the system will evolve to a state where the third output port has the high output power. In Figure 5, the switching is done between the three possible output states. The time is expressed in units of the characteristic lifetime τ of the cavity. A constant input power of $3.3P_0$ is injected in the three cavities. To achieve switching, this input power is increased in two of the three input ports to $3.5P_0$ during a time 30τ.

We do the same for the bifurcation diagram of Figure 2b. We work in the same regime as before and find that by injecting a single pulse in one of the output ports, the system switches to a state where that output is high and the other outputs low. This is demonstrated for an input power of 0.5 P_0 which is increased to 1.2 P_0 in case of a pulse (Figure 5b). We observed robust switching behaviour: small variations on the input power do not cause switching and a variation of 30% on the values of Δ of the different cavities is possible when using higher pulse powers.

[Fig. 5 about here.]

The switching times scale with the Q-factor of the cavity. If we assume the cavity has a Q-factor of 4000, the switching time can be predicted to be 520 ps. This rather slow switching speed is due the fact that the system has to travel over a large distance in phase space. It can be reduced by also adjusting the phase of the injected pulses, as demonstrated for a single cavity in [14]. The energy needed to enter the bistable regime is proportional to the Kerr-nonlinearity and becomes lower if the mode has a small volume. In literature, we find typically a value of 2.6 mW for photonic crystal cavities [15]. In silicon ring resonators with a Q-factor of 14 000 an operational value of about 6 mW is necessary [12]. Two possible suggestions for a practical implementation of the proposed scheme are depicted in Figure 6 as an illustration: the first using a photonic crystal cavity with a hexagonal symmetry in the cavity mode and the other consisting of ring resonators coupled to waveguides.

[Fig. 6 about here.]

3. Four coupled cavities

3.A. Symmetry breaking conditions

The analysis for the symmetric structure of four coupled cavities (Figure 7) is similar to the previous one.

[Fig. 7 about here.]

The time dependance of the resonant modes of the cavities is now:

$$\frac{\mathrm{d}a_1}{\mathrm{d}t} = \left[i\left(\omega_0 + \delta\omega_1\right) - \frac{1}{\tau}\right] a_1 + df_1 + db_5 + df_8 \tag{18}$$

$$\frac{\mathrm{d}a_2}{\mathrm{d}t} = \left[i\left(\omega_0 + \delta\omega_2\right) - \frac{1}{\tau}\right] a_2 + df_2 + db_6 + df_5 \tag{19}$$

$$\frac{\mathrm{d}a_3}{\mathrm{d}t} = \left[i\left(\omega_0 + \delta\omega_3\right) - \frac{1}{\tau}\right] a_3 + df_3 + db_7 + df_6 \tag{20}$$

$$\frac{\mathrm{d}a_4}{\mathrm{d}t} = \left[i\left(\omega_0 + \delta\omega_4\right) - \frac{1}{\tau}\right] a_4 + df_4 + db_8 + df_7 \tag{21}$$

By using the same definitions as before and equations (6-7), we rewrite these in the following form:

$$\left[i\left(\omega_0-\omega+\delta\omega_1\right)-\frac{1}{\tau}\right]a_1+\kappa\left(2\gamma a_1+a_2+a_4\right) = -df_1 \quad (22)$$

$$\left[i\left(\omega_0-\omega+\delta\omega_2\right)-\frac{1}{\tau}\right]a_2+\kappa\left(2\gamma a_2+a_1+a_3\right) = -df_2 \quad (23)$$

$$\left[i\left(\omega_0-\omega+\delta\omega_3\right)-\frac{1}{\tau}\right]a_3+\kappa\left(2\gamma a_3+a_4+a_2\right) = -df_3 \quad (24)$$

$$\left[i\left(\omega_0-\omega+\delta\omega_4\right)-\frac{1}{\tau}\right]a_4+\kappa\left(2\gamma a_4+a_3+a_1\right) = -df_4 \quad (25)$$

To find a condition for symmetry breaking, it is assumed that all inputs are equal ($f_1 = f_2 = f_3 = f_4$). By combining the first and the third equation, we obtain an equation similar to equation 12:

$$\left[-\frac{1}{3}+i\left(\Delta''+A\right)\right]a_1=\left[-\frac{1}{3}+i\left(\Delta''+C\right)\right]a_3 \quad (26)$$

with

$$\Delta''=\Delta-\frac{2}{3}\cot\phi \quad (27)$$

The same relation can be derived for B and D when combining the second and the fourth equation.

When we apply the same reasoning as in the previous case of 3 coupled cavities, we find the following condition for symmetry breaking with a self-focusing Kerr effect (positive nonlinearity):

$$\Delta''>\frac{1}{\sqrt{3}} \quad (28)$$

In Figure 8 the conditions for 3 and 4 coupled cavities are depicted graphically as a function of Δ and ϕ.

[Fig. 8 about here.]

3.B. Static solutions

We can solve the coupled-mode equations again under steady state conditions and perform a stability analysis which takes now a Jacobian matrix of 64 elements to be evaluated at each point. We can depict the stable output powers as a function of the input power for a configuration where the symmetry breaking condition is fulfilled, see Figure 9. In this configuration, there are two different asymmetric solutions. The first one to show up has a left-right symmetry with two pairs of equal output power (e.g. $A = B$ and $C = D$). In the next solution, two opposing cavities have the same output power and the other two outputs are respectively higher and lower (e.g. $A = C$ and $B < A < D$). By increasing the detuning a whole range of other states can be found, resulting in very complex state diagrams.

[Fig. 9 about here.]

When analyzing the energy in the cavities, we observe a similar behaviour as in Figure 3 where we have a bifurcation in the symmetric solution which becomes unstable in the lower branch.

3.C. Dynamic behaviour

As demonstrated in Figure 10, we can again switch between the different states by injecting pulses. We describe in more detail the solution with two pairs of equal output. By injecting a short pulse in a port with a high output, that output becomes low and the port at the opposite side will become high. We inject the pulses by increasing the input power from 1.2 P_0 till 1.4 P_0 during a period of 5τ. A cyclical switching action ensues: the state rotates as a result of the switching pulse.

[Fig. 10 about here.]

4. Conclusion

We demonstrated analytically and numerically symmetry breaking in structures composed of 3 and 4 cavities. Intricate bifurcation behavior with different regimes is uncovered and dynamical studies demonstrate multi-stable and cyclical flip-flop operation. With currently hundreds of coupled cavities being studied experimentally in the linear regime [4], nonlinear dynamics in smaller networks are the logical next step.

5. Acknowledgments

This work is supported by COST Action MP0702 and the interuniversity attraction pole (IAP) "Photonics@be" of the Belgian Science Policy Office. K. Huybrechts acknowledges the Institute for the Promotion of Innovation through Science and Technology (IWT) for a specialization grant. B. Maes acknowledges the Fund for Scientific Research (FWO) for a post-doctoral fellowship.

References

1. K. Vandoorne, W. Dierckx, B. Schrauwen, D. Verstraeten, R. Baets, P. Bienstman, and J. Van Campenhout, "Toward optical signal processing using photonic reservoir computing," Optics Express, **16**(15), 11182–11192 (2008).
2. M. Soljacic, S. G. Johnson, S. H. Fan, M. Ibanescu, E. Ippen, and J. D. Joannopoulos, "Photonic-crystal slow-light enhancement of nonlinear phase sensitivity," Journal of the Optical Society of America B, **19**(9), 2052-2059 (2002).

3. B. Maes, M. Soljacic, J. D. Joannopoulos, P. Bienstman, R. Baets, S. P. Gorza, and M. Haelterman. "Switching through symmetry breaking in coupled nonlinear microcavities," Optics Express, **14**(22), 10678–10683 (2006).
4. M. Notomi, E. Kuramochi, and T. Tanabe, "Large-scale arrays of ultrahigh-Q coupled nanocavities," Nature Photonics, **2**(12), 741–747 (2008).
5. O. D'Huys, R. Vicente, T. Erneux, J. Danckaert, and I. Fischer, "Synchronization properties of network motifs: Influence of coupling delay and symmetry," Chaos, **18**(3), 11 (2008).
6. B. Maes, P. Bienstman, and R. Baets, "Symmetry breaking with coupled fano resonances," Optics Express, **16**(5), 3069–3076 (2008).
7. S. X. Zhang, D. Owens, Y. Liu, M. Hill, D. Lenstra, A. Tzanakaki, G. D. Khoe, and H. J. S. Dorren, "Multistate optical memory based on serially interconnected lasers," Photonics Technology Letters, **17**(9), 1962–1964 (2005).
8. S. Zhang, D. Lenstra, Y. Liu, H. Ju, Z. Li, G. D. Khoe, and H. J. S. Dorren, "Multi-state optical flip-flop memory based on ring lasers coupled through the same gain medium," Optics Communications, **270**(1), 85–95 (2007).
9. P. E. Barclay, K. Srinivasan, and O. Painter, "Nonlinear response of silicon photonic crystal microresonators excited via an integrated waveguide and fiber taper," Optics Express, **13**(3), 801–820 (2005).
10. M. Notomi, A. Shinya, S. Mitsugi, G. Kira, E. Kuramochi, and T. Tanabe, "Optical bistable switching action of si high-Q photonic-crystal nanocavities," Optics Express, 13(7), 2678–2687 (2005).
11. T. Uesugi, B. S. Song, T. Asano, and S. Noda, "Investigation of optical nonlinearities in an ultra-high-q si nanocavity in a two-dimensional photonic crystal slab," Optics Express, **14**(1),377–386 (2006).
12. Q. F. Xu and M. Lipson, "Carrier-induced optical bistability in silicon ring resonators," Optics Letters, **31**(3),341–343 (2006).
13. G. Roelkens, L. Liu, D. Van Thourhout, R. Baets, R. Notzel, F. Raineri, I. Sagnes, G. Beaudoin, and R. Raj, "Light emission and enhanced nonlinearity in nanophotonic waveguide circuits by III-V/silicon-on-insulator heterogeneous integration," Journal of Applied Physics, **104**(3),7 (2008).
14. H. Kawashima, Y. Tanaka, N. Ikeda, Y. Sugimoto, T. Hasama, and H. Ishikawa, "Numerical study of impulsive switching of bistable states in nonlinear etalons," IEEE Photonics Technology Letters, **19**(9-12), 913–915 (2006).
15. M. Soljacic, M. Ibanescu, S. G. Johnson, Y. Fink, and J. D. Joannopoulos, "Optimal bistable switching in nonlinear photonic crystals," Physical Review E, **66**(5), 055601 (2002).

16. S. H. Fan, W. Suh, and J. D. Joannopoulos, "Temporal coupled-mode theory for the fano resonance in optical resonators," *Journal of the Optical Society of America A - Optics Image Science and Vision*, **20**(3), 569–572 (2003).
17. B. Maes, P. Bienstman, and R. Baets, "Switching in coupled nonlinear photonic-crystal resonators," Journal of the Optical Society of America B-Optical Physics, **22**(8), 1778–1784 (2005).

List of Figures

1 A schematic representation of a symmetric structure of three coupled cavities. 12
2 The states of the output power as a function of the input power for a structure with (a) $\Delta = 0.1$ and $\phi = -0.5$ and (b) $\Delta = 0.1$ and $\phi = 2.0$. The unstable states are shaded. 13
3 The stable states of the cavity energies as a function of the input power for a structure with $\tau(\omega - \omega_0) = 0.1$ and $\phi = -0.5$. The unstable states of the symmetric solutions are shaded. 14
4 The different working regimes for different parameters of Δ and ϕ with a constant input power of $P_{in}/P_0 = 3.0$. I: two equal solutions in the upper branch and one in the lower branch (bounded by orange line); II: three different outputs (bounded by blue line); III: two equal solutions in the lower branch and one in the higher branch (bounded by brown line). The cross indicates the working point of Figure 2a. 15
5 Switching between the three different states of region III. 16
6 Two possible implementations of the proposed scheme using (a) photonic crystal cavities and (b) ring resonators. 17
7 Schematic representation of a symmetric structure of 4 cavities coupled by waveguides. 18
8 Schematic representation of the symmetry breaking condition for 3 and 4 coupled cavities. In the dark regions, the symmetry breaking condition holds. 19
9 Stable states of the output power as a function of the input power for a structure consisting of 4 cavities with $\Delta = -0.35$ and $\phi = 0.6$. The unstable states are plotted with a thin line. 20
10 Switching between different states in a configuration of 4 cavities. 21

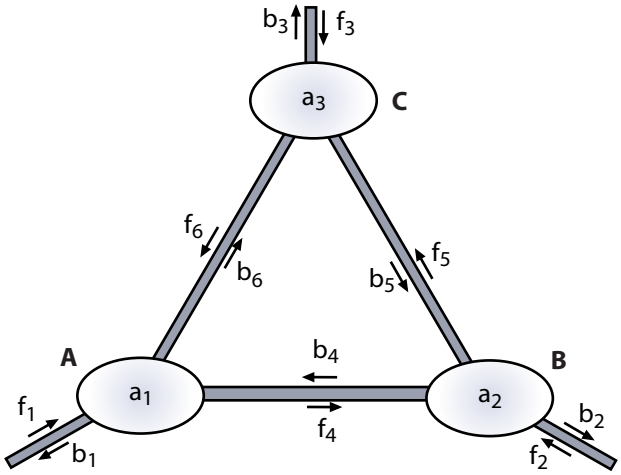

Fig. 1. A schematic representation of a symmetric structure of three coupled cavities.

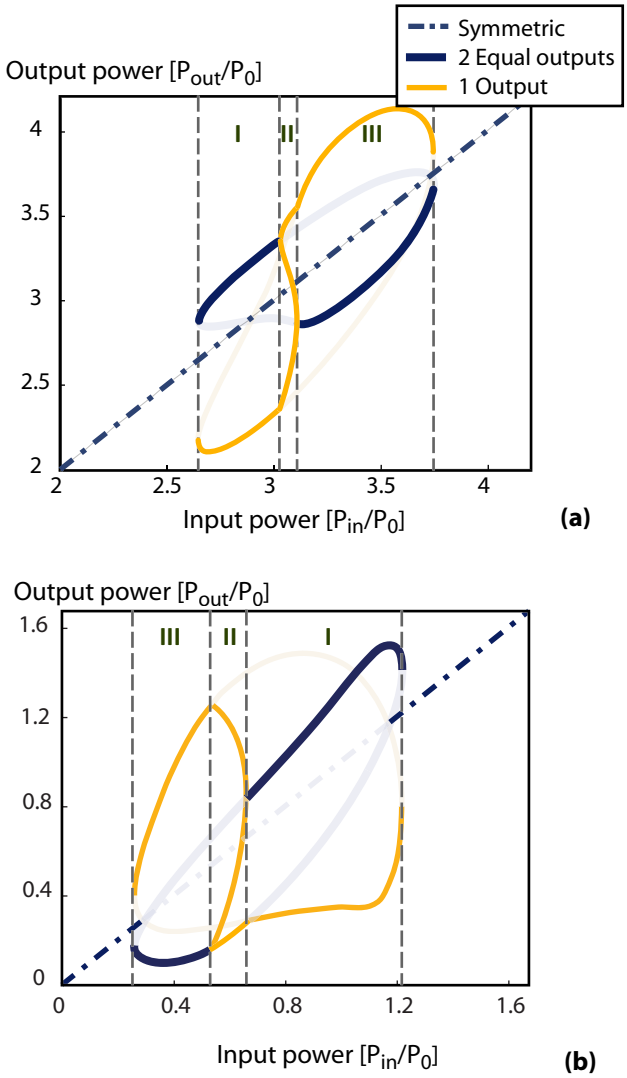

Fig. 2. The states of the output power as a function of the input power for a structure with (a) $\Delta = 0.1$ and $\phi = -0.5$ and (b) $\Delta = 0.1$ and $\phi = 2.0$. The unstable states are shaded.

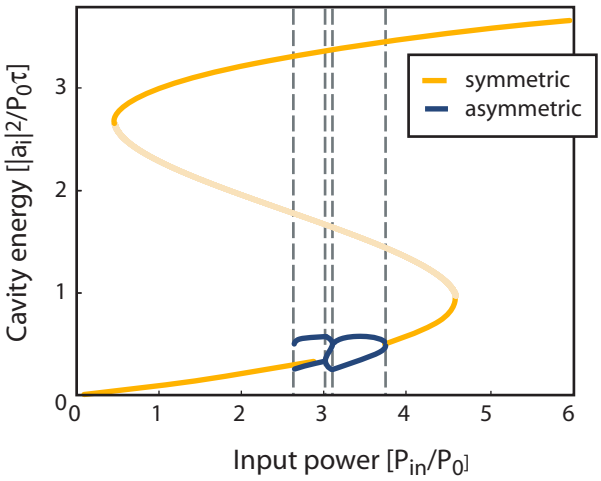

Fig. 3. The stable states of the cavity energies as a function of the input power for a structure with $\tau(\omega - \omega_0) = 0.1$ and $\phi = -0.5$. The unstable states of the symmetric solutions are shaded.

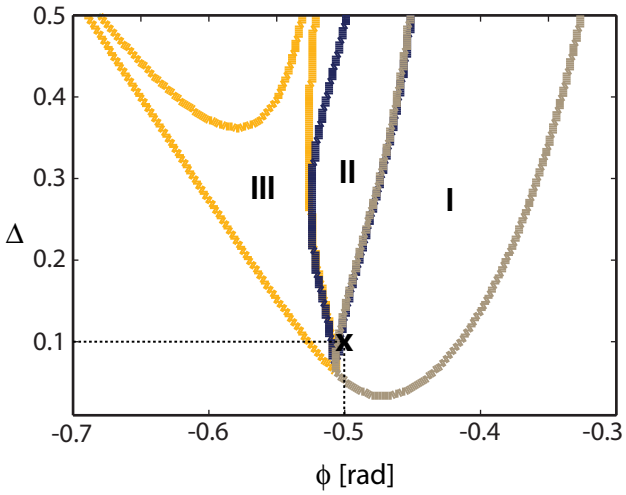

Fig. 4. The different working regimes for different parameters of Δ and ϕ with a constant input power of $P_{in}/P_0 = 3.0$. I: two equal solutions in the upper branch and one in the lower branch (bounded by orange line); II: three different outputs (bounded by blue line); III: two equal solutions in the lower branch and one in the higher branch (bounded by brown line). The cross indicates the working point of Figure 2a.

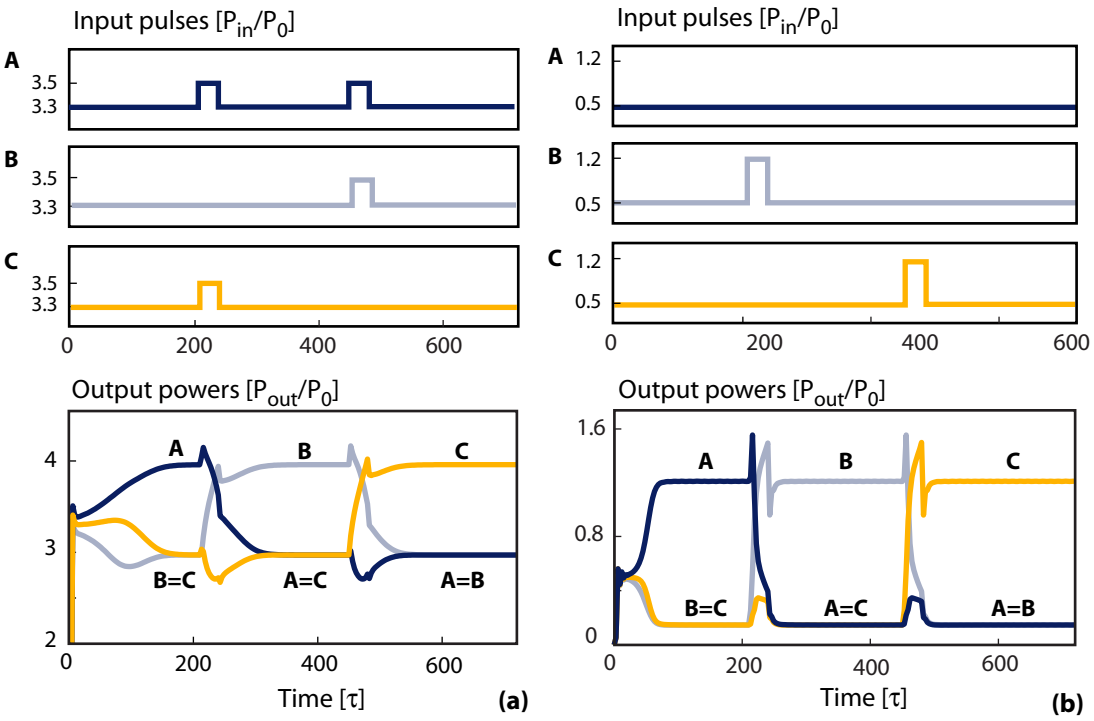

Fig. 5. Switching between the three different states of region III.

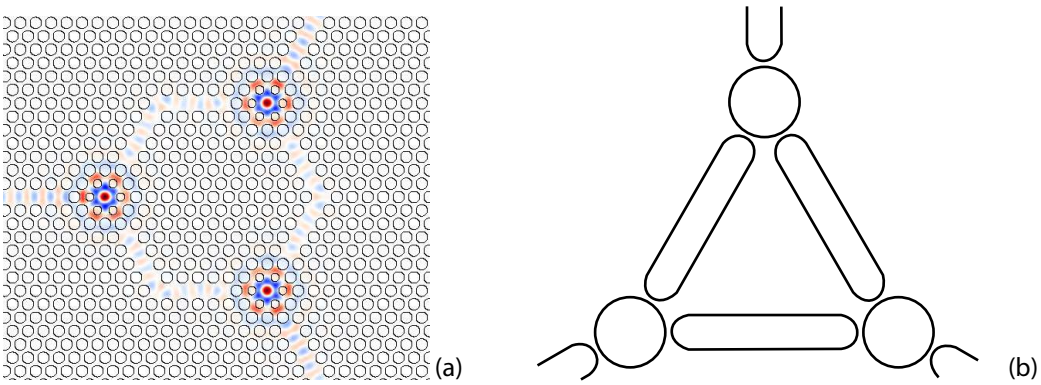

Fig. 6. Two possible implementations of the proposed scheme using (a) photonic crystal cavities and (b) ring resonators.

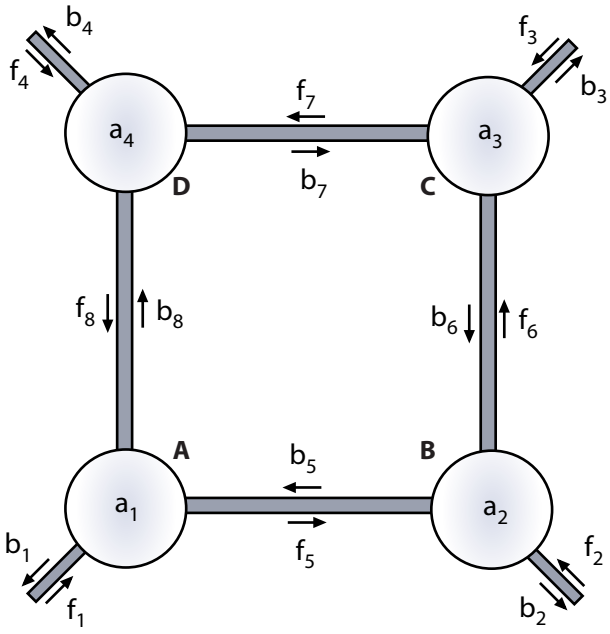

Fig. 7. Schematic representation of a symmetric structure of 4 cavities coupled by waveguides.

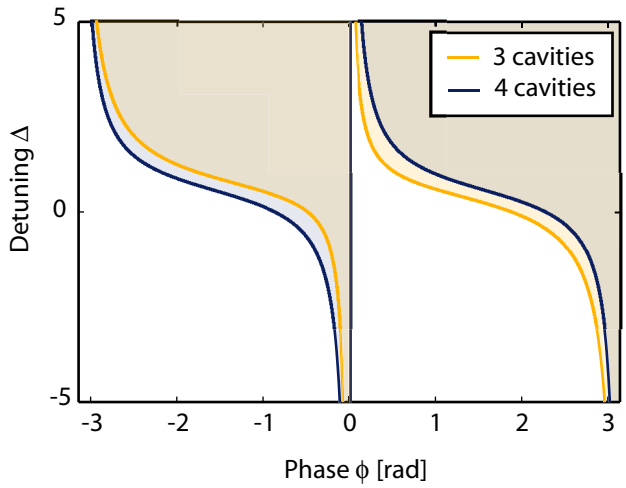

Fig. 8. Schematic representation of the symmetry breaking condition for 3 and 4 coupled cavities. In the dark regions, the symmetry breaking condition holds.

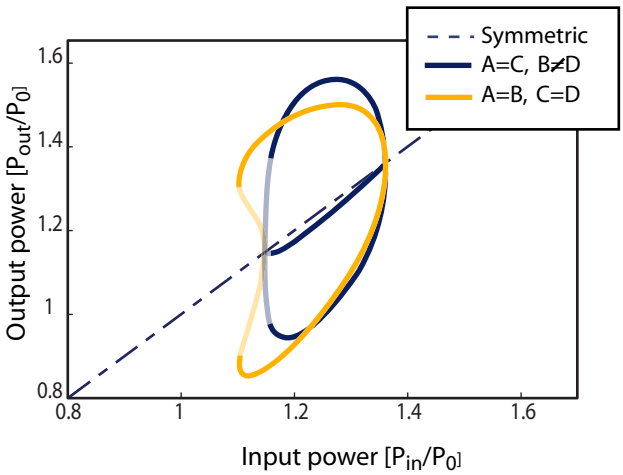

Fig. 9. Stable states of the output power as a function of the input power for a structure consisting of 4 cavities with $\Delta = -0.35$ and $\phi = 0.6$. The unstable states are plotted with a thin line.

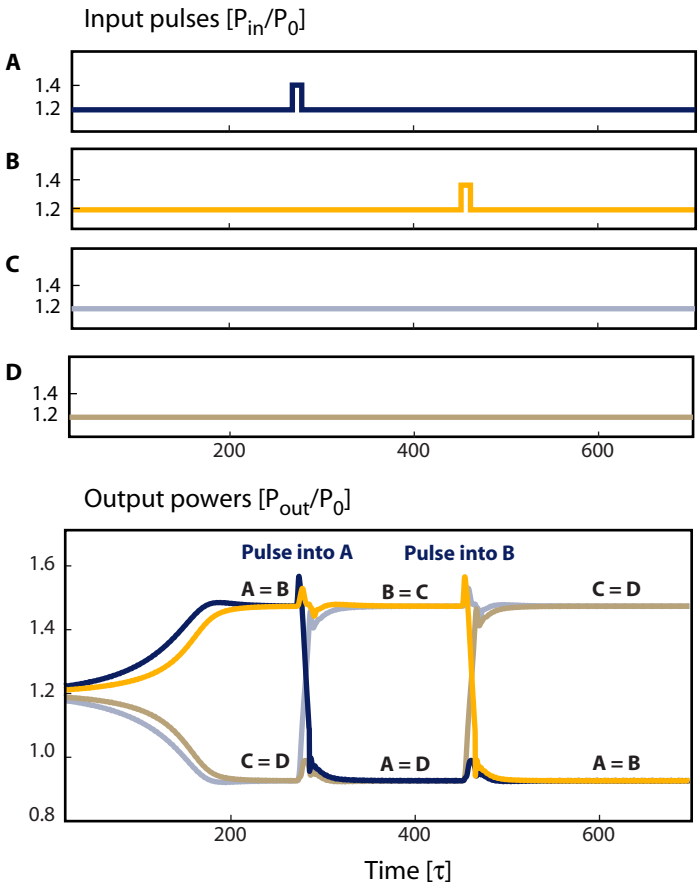

Fig. 10. Switching between different states in a configuration of 4 cavities.